Heliyon 10 (2024) e24331

Contents lists available at ScienceDirect

Heliyon

journal homepage: www.cell.com/heliyon

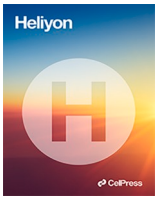

Research article

Direct numerical simulation of contaminant removal in presence of underfloor air distribution system

Yaowen Xia *, Saidong Lyu

Key Laboratory of Rural Energy Engineering of Yunnan and Solar Energy Research Institute, Yunnan Normal University, Kunming, Yunnan, 650092, China

ARTICLE INFO

Keywords:
Ventilation effectiveness
Contaminant removal
COVID-19
Direct numerical simulation

ABSTRACT

Indoor contaminant removal over $0.5 \leq FrT \leq 5.0$, $0.5 \leq N \leq 5.0$, and $50 \leq Re \leq 500$ was investigated numerically, wherein Fr_T refers to the Froude number, N refers to the buoyancy ratio, and Re refers to the Reynolds number. As demonstrated, the ventilation effectiveness increased with increasing contaminant source intensity and air supply intensity at a constant air temperature, indicating that increase the fresh air can effectively eliminate contaminants in this case. At high air supply temperatures, the heat retention time and contaminant transport was extremely short, and the fresh air induced by strong natural convection floating lift was rapidly discharged. Additioanlly, the air supply intensity had significant effects on contaminant removal. Quantification of the ventilation effectiveness under the combined effects of air supply intensity, air supply temperature and contaminant source intensity was determined based on the results of direct numerical simulations.

1. Introduction

Indoor air pollution is hazardous to the human immune systems, causing the body to be more vulnerable to viral diseases in the era of COVID-19 pandemic. Therefore, appropriate indoor ventilation is essential to reduce concentrations of air pollutants and improve air quality [1,2]. The underfloor air distribution (UFAD) system generates fresh air via the floor air vent, thereby reducing the contaminant concentration and improve indoor air quality [3].

Nowadays, human typically spend 90 % of their time indoor, while natural ventilation is not sufficient to guarantee indoor air quality [4]. An appropriate ventilation system can not only facilitate the control of indoor temperature and humidity, but also remove indoor pollutants. The ventilation system mainly considers the rationality of indoor airflow distribution and different air distributions lead to different ventilation modes [5]. Meanwhile, the indoor pollutant concentrations can be several times higher than outdoor pollutant concentrations. Inappropriate indoor air flow would severely affect human health and may cause increased building energy consumption [6–8]. It has been demonstrated that indoor airflow play a key role in air quality and pollution control.

The UFAD systems can achieve rational indoor air quality at low costs. It has been the focus in the field of air conditioning over the past decades [9,10]. Indeed, the UFAD system injects fresh air into the room via the ventilation inlet on the floor, and the air pollutants are discharged from the air outlets [11].

The UFAD system was first used for cooling of computer rooms in the 1950s and subsequently introduced in the West German

* Corresponding author.
E-mail address: yaowenxia@ynnu.edu.cn (Y. Xia).

https://doi.org/10.1016/j.heliyon.2024.e24331
Received 27 June 2023; Received in revised form 7 December 2023; Accepted 7 January 2024
Available online 12 January 2024

Foreign Office building in the 1970s [12]. Numerical simulation of heat and mass transport of indoor airflow is a critical to understand and evaluate the indoor air quality. By analyzing the indoor ventilation strategies (e.g., mixed ventilation, UFAD and displacement ventilation), indoor air quality and CO_2 concentration can be determined [13–15], as air velocity field, temperature field and pollutant distribution under different ventilation modes can be simulated. A series of working condition simulations based on different parameters and analysis of personal have been reported, including the correlation of air temperature and personal comfort [16–20]. Alajmi et al. [21] found that any inhabited room can be divided into the cold zone at the bottom, the narrower zone in the lower part, the transition zone and the upper warm zone. Meanwhile, the room height also affects air stratification. Tsai et al. [22] reported that the impacts of air temperature on the vertical distribution of temperature were negligible, and the vertical momentum had a positive correlation with the temperature in the lower part; as the airflow increased, temperature stratification induced by the increased supply of air momentum decreased. Ismail et al. [23] investigated the thermal performance of UFAD in rooms with one and two occupants using Computational Fluid Dynamics (CFD), and the results (e.g., distributions of airflow velocity and temperature, energy consumption and comfort) were compared with the top air distribution systems. Additionally, position and height of heat source and intensity of heat supply would greatly affect temperature stratification and personal comfort [24]. UFAD systems were numerically simulated in a large space with air supply intensity and the position of ventilation inlet as the variables [25,26]. The results showed that requirements on the personal comfort can be satisfied under all working conditions involved.

Indoor airflow structure is one of the most important physical parameters of the indoor air. Indeed, personal comfort is directly dependent on the rationality of indoor airflow structure. The indoor air is mainly reflected by a mixed process of air flow and heat/pollutant transmission, including air convection heat transfer and mass transfer. Therefore, improvement of indoor air quality can only be achieved based on full understanding of the transport and diffusion of indoor heat and pollutants under different conditions. In presence of both temperature gradients and concentration gradients, natural convection with double buoyancy may be observed. Concentration and temperature gradients generate concentration and thermal buoyancy, respectively. The magnitude, direction, and relative position of temperature and concentration gradients have direct impacts on natural convective heat transfer and mass transfer. Additionally, the interaction (coupling effect) of heat and mass transfer was also observed for indoor air. The concentration field (or the temperature field) affects the flow field, which in turn affects the temperature field (or the concentration field), indicating an indirect correlation of the concentration field and the temperature field; complex fluid flow conditions tend to be observed due to variations of thermal diffusion rate and solute diffusion rate. With the widespread of UFAD systems in recent years, both heat and pollutant buoyancy shall be taken into consideration. Although this phenomenon has been observed for a long time, various problems about the fluid transportation mechanism in presence of both temperature and concentration gradients remain to be solved. Theoretical analysis, as well as numerical simulation and experimental methods, has been widely employed for such problems. Lin et al. [27] proposed a model of UFAD systems comprising one heat source and one ventilation outlet and verified by experiments. The results showed that parameters influencing airflow include thermal buoyancy flux, volume energy and momentum. This model was established base on the flow fountain model and the heat source plume. Liu et al. [28] proposed models with multiple ventilation inlets and one heat source floor at different levels. The experimental results showed that the fluid flow is mainly determined by the entrainment and negative buoyancy jet entering the plume. A theoretical model based on stratified ventilation was established and the results obtained by this model were compared with the experimental results. Lin et al. [29] demonstrated that as the ventilation volume of the UFAD system increased, the gradient slope of vertical temperature and the stratified height increased. Kanaan [30] proposed simulation of UFAD systems with multiple ventilation inlets and multiple heat sources from both theoretical and CFD perspectives. The results showed that the CO_2 concentration predicted by theoretical analysis was consistent with that obtained by the CFD.

Ventilation effectiveness is a critical evaluation index reflecting the indoor discharging effect [31,32]. It is usually employed as an indoor air quality indicator for the design of heating ventilation, especially in cases with known pollutant concentrations [33–35]. In recent years, studies of thermal comfort focused on parameters such as predicted mean vote (PMV), percentage of dissatisfaction (PPD), ventilation efficiency and the feeling of blowing. CFD is a feasible method to evaluate indoor air quality from a microscopic perspective and facilitate the control of pollutant distribution and diffusion. Indeed, a comprehensive analysis of the indoor temperature field, velocity field and PMV/PPD is essential for development of optimized indoor air quality [36,37]. Cheong et al. [10] investigated the effects of underfloor ventilation system and traditional mixed ventilation system in a primary school on elimination of airborne pathogens. The results demonstrated that the vent shall be installed away from the breathing area. Fan et al. [38] thoroughly investigated different ventilation modes during the outbreak of COVID-19, aiming to improve thermal comfort, air quality and virus elimination, the thermal comfort, ventilation efficiency and discharging efficiency under different ventilation modes in different situations were assessed. Gao et al. [39] explored the influences of surface temperature of ceiling and air velocity on indoor air pollutant distribution. The vertical distribution of indoor air temperature, wind speed, pollutant concentration and discharging effect were investigated, respectively. The results showed that the surface temperature of ceiling had negligible effects on the vertical distribution of air pollutants, while the air supply intensity had significant influences on indoor air pollutant distribution and the discharging effect. Zhang et al. [40] focused on the thermal stratification of UFAD system, and obtained characteristic parameters of the horizontal, dimensionless temperature distribution between the ankle and head by using multivariable regression analysis.

To the best of our knowledge, few studies on UFAD system using Direct Numerical Simulation (DNS) have been reported, and the influences of the air supply temperature, air supply intensity and contaminant source intensity remain unclear. This study aims to deepen the understanding of the effectiveness of pollutant removal in a room with a UFAD system.

This paper is organized as follows: Section 2 briefly describes the physical model, the numerical methodology, mesh generation and the results of time-step independence test, as well as the DNS results were introduced in Section 3.Section 4 presents a description of the evolution of typical thermal-solutal contours based on the DNS results, along with the pollutant source intensity, the air supply temperature and quantitative analysis of the air supply intensity. The conclusions are given in Section 5.

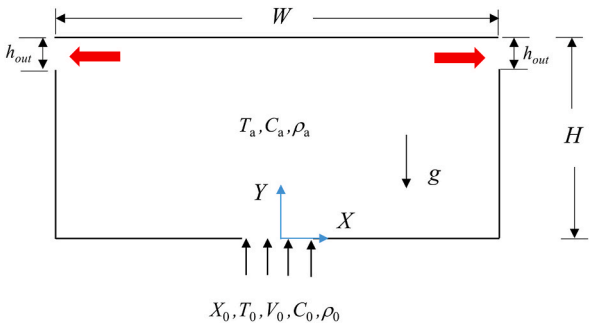

Fig. 1. The physical and numerical models.

2. Numerical methodology and numerical simulations

Fig. 1 shows a 2D rectangular domain (height = H, width = W) representing a physical system and corresponding numerical. Herein, the origin of the 2D cylindrical coordinate system (*X*, *Y*) is located at the floor center. The working fluid is an air-pollutant mixture. Meanwhile, the ambient fluid is a Newtonian one, which is initially stationary under a uniform temperature (T_a) and a uniform concentration (*Ca*). At the center of the floor ($Y = 0$), the radius of the fluid is X_0. The remaining floor is an essentially rigid, insulated and stationary boundary. At t = 0, a fresh air jet with temperature of T_0 ($T_0 < T_a$) and pollutant concentration of C_0 is injected into the domain at a uniform rate (V_0) to trigger the air flow and exits naturally from the air outlet port at the top of the side walls.

The flow of air-pollutant in a room is governed by the 2D incompressible Navier-Stokes (*N*–S) equations. The buoyancy was determined by the Oberbeck-Boussinesq approximation, with the gravity along the negative *Y* (vertical) direction.

The density of fluid at *T* and *C*, $\rho(T, C)$, can be determined by:

$$\rho(T, C) = \rho_a(T_a, C_a)[1 - \beta_T(T - T_a) - \beta_C(C - C_a)] \tag{1}$$

where $\rho_a(T_a, C_a)$ refers to the initial density of the ambient fluid at *Ta* and *Ca*, and β_T and β_C are the volumetric thermal and mass expansion coefficients of the fluid, respectively.

Re, Fr_T, *Sc* , and *N* are defined as (equation (2) and (3)) follows:

$$Re = \frac{V_0 X_0}{\nu}, Fr_T = \frac{V_0}{\sqrt{g\beta_T(T_a - T_0)X_0}}, Sc = \frac{\nu}{D} \tag{2}$$

$$N = \frac{\beta_C(C_a - C_0)}{\beta_T(T_a - T_0)} \tag{3}$$

N denotes the influences of concentration on density in comparison with temperature, ν is kinematic viscosity, and D is the diffusivity.

The overall ventilation effectiveness for temperature distribution ε_t serves as a quantitative indicator associated with the heat distribution inside the cavity, and the effectiveness for pollutant removal, ε_c, serves as a quantitative indicator associated with the pollutant distribution inside the cavity [41]. Herein, the two parameters are defined as follows (equation (4) and (5)):

$$\varepsilon_t = \frac{T_{out} - T_0}{T_{average} - T_0} \tag{4}$$

$$\varepsilon_c = \frac{C_{out} - C_0}{C_{average} - C_0} \tag{5}$$

where T_{out} and C_{out} are the average temperature and average pollutant concentration at the outlet, respectively, $T_{average}$ and $C_{average}$ are the average temperature and average pollutant concentration inside the cavity, respectively, T_0 and C_0 are the average temperature and average pollutant concentration at the inlet, respectively.

2.1. Mesh generation and bench marking of numerical simulation

To keep the numerical simulation independent from time step and grid, we conducted a series of independent tests. Fig. 2 shows the results of grid and time-step independent tests with $Pr = 0.71$, $Ra_T = 3.0 \times 10^8$, $Le = 1.0$, $N = -1$, $Re = 300$, and $Fr_T = 0.5$. Herein, the vertical profile of velocity, overall ventilation effectiveness in terms of temperature distribution and the pollutant removal were demonstrated. Three different meshes (1.05695 million meshes, 1.62104 million meshes, and 2.18026 million meshes) (Fig. 2a–c) and three different time steps (0.01s, 0.025s, and 0.05s) (Fig. 2d–f) were involved. As indicated, the DNS results with different meshes but constant time step (0.025 s) were identical. The DNS results with different time steps but constant mesh (1.62104 million meshes) were

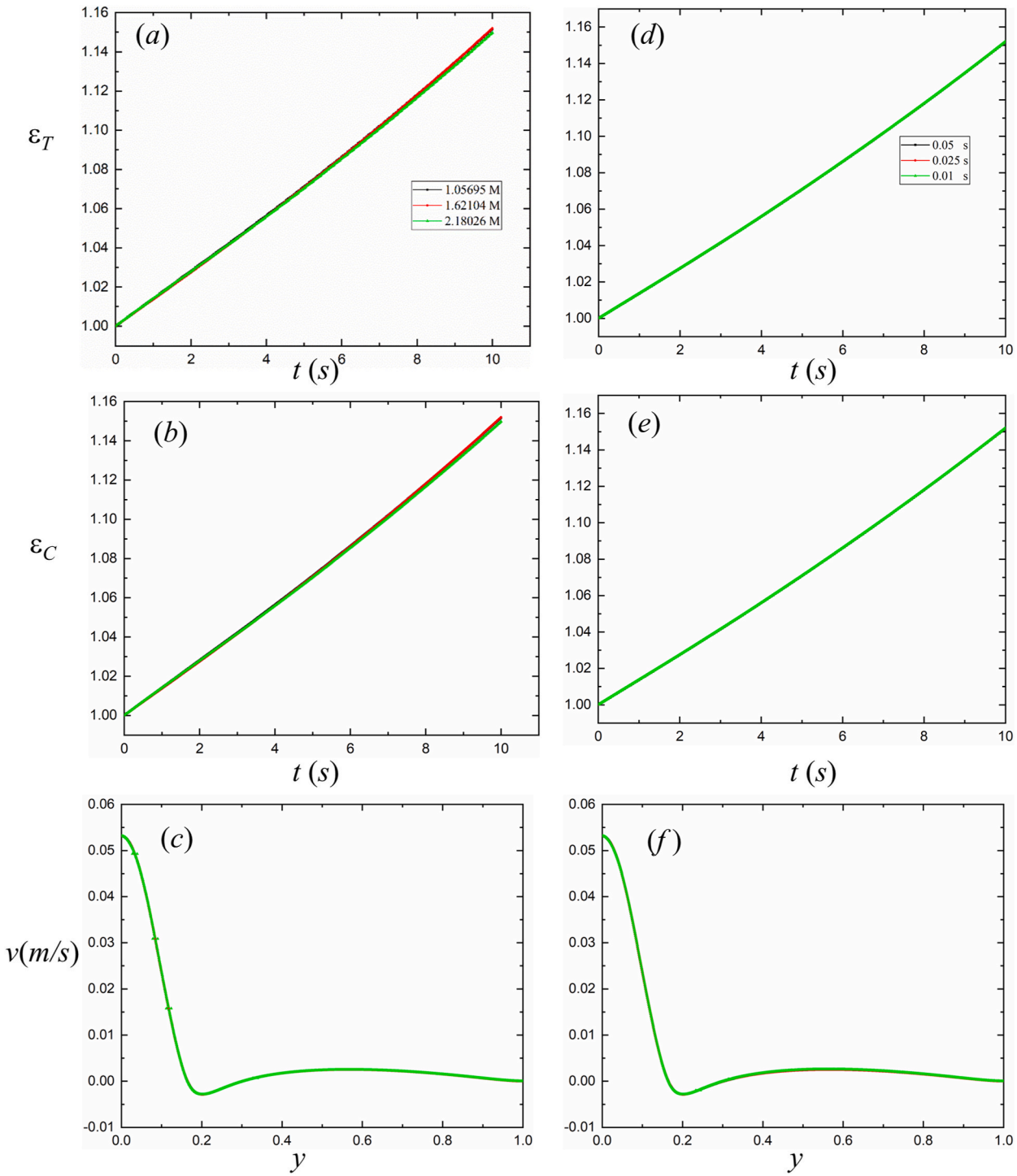

Fig. 2. DNS results in cases of different meshes (left column) and different steps (right column): ventilation effectiveness for temperature distribution (top row), ventilation effectiveness for pollutant removal (middle row), and vertical profiles of velocity (bottom row).

also identical. It was found that 1.62104 million meshes and a time step of 0.025 s were employed for all DNS cycles in this study as they can deliver numerical simulation results with sufficiently high accuracy.

The ANSYS Fluent code used for DNS cycles were bench marked to guarantee that the accuracy was sufficiently high. Indeed, a numerical code requires verification and validation using data available. Specifically, the subject of several works of numerical validations was selected for code benchmarking [42–45]. Additionally, the cavity is heated differentially with adiabatic horizontal walls.

Table 1
Num in the case of $Ra_T = 7.0 \times 10^9$, Pr = 0.71, $Le = 1.0$.

N	Present study	Sezai [46]	Koufi L [47]	Xamán [48]	Béghein [49]
−0.01	16.6	16.3	13.4	16.6	16.4
−0.1	16.0	15.9	16.0	15.9	16.0
−0.2	15.5	15.4	15.3	15.4	15.5
−0.5	13.6	13.5	13.6	13.6	13.6
−0.8	10.7	10.5	10.6	10.6	10.6
−0.9	8.9	8.6	8.8	8.8	8.8
−1.5	13.7	13.5	13.5	13.6	13.6
−5.0	23.7	23.7	23.7	23.7	23.7

Table 2
Key data of the DNS runs.

Runs	*N*	Fr_T	*Re*	*Fr*	V_0 *(m/s)*	Qs (L/s.m^2)	ΔT *(K)*	ΔC *(%)*
1	3.0	2.0	50	1.0	0.02658	7.51×10^{-5}	0.180231	0.005296
2	3.0	2.0	100	1.0	0.053161	1.50×10^{-4}	0.720926	0.021182
3	3.0	2.0	200	1.0	0.106322	3.00×10^{-4}	2.883703	0.08473
4	3.0	2.0	300	1.0	0.159483	4.51×10^{-4}	6.488331	0.190642
5	3.0	2.0	500	1.0	0.265805	7.51×10^{-4}	18.02314	0.529562
6	3.0	0.5	100	0.3	0.053161	1.50×10^{-4}	11.53481	0.33892
7	3.0	1.0	100	0.5	0.053161	1.50×10^{-4}	2.883703	0.08473
8	3.0	1.5	100	0.8	0.053161	1.50×10^{-4}	1.281646	0.037658
9	3.0	3.0	100	1.5	0.053161	1.50×10^{-4}	0.320411	0.009414
10	3.0	5.0	100	2.5	0.053161	1.50×10^{-4}	0.115348	0.003389
11	0.5	0.5	100	0.4	0.053161	1.50×10^{-4}	11.53481	0.056487
12	0.5	1.0	100	0.8	0.053161	1.50×10^{-4}	2.883703	0.014122
13	0.5	1.5	100	1.2	0.053161	1.50×10^{-4}	1.281646	0.006276
14	0.5	2.0	100	1.6	0.053161	1.50×10^{-4}	0.720926	0.00353
15	0.5	3.0	100	2.4	0.053161	1.50×10^{-4}	0.320411	0.001569
16	0.5	5.0	100	4.1	0.053161	1.50×10^{-4}	0.115348	0.000565
17	0.1	2.0	100	1.9	0.053161	1.50×10^{-4}	0.720926	0.000706
18	1.0	2.0	100	1.4	0.053161	1.50×10^{-4}	0.720926	0.007061
19	1.5	2.0	100	1.3	0.053161	1.50×10^{-4}	0.720926	0.010591
20	2.0	2.0	100	1.2	0.053161	1.50×10^{-4}	0.720926	0.014122
21	5.0	2.0	100	0.8	0.053161	1.50×10^{-4}	0.720926	0.035304
22	10.0	2.0	100	0.6	0.053161	1.50×10^{-4}	0.720926	0.070608

To achieve that, it was set that $Pr = 0.71$, $Ra_T = 10^7$, $Le = 1$. Table 1 lists the average Nusselt number *Num*, which is defined by:

$$Num = \int_0^1 (Nu_L)_{X=0} dY = \int_0^1 (-\partial\theta/\partial X)_{X=0} dY \tag{6}$$

As demonstrated, the accuracy of ANSYS Fluent code is sufficiently high for direct numerical simulation of pollutant removal in a room with underfloor air distribution systems.

2.2. Numerical simulations

A total of 22 DNS runs (see Table 2 for details) were executed using ANSYS Fluent 2020 R2. Air mixture was employed as the fluid in DNS, wherein $\rho_a = 1.16 kg/m^3$, kinematic viscosity $\nu = 1.85 \times 10^{-5}$ m^2/s, $\beta_T = 3.33 \times 10^{-3}$ $1/K$, $\beta_C = -0.34$ 1/(%), Pr = 0.71, and $Le = 1.0$. As observed, parameters reflecting the air intensity, the air temperature and the pollutant intensity were Fr_T, Re and *N*, which varied in the ranges of 0.5–5.0, 50–500 and 0.1–10.0, respectively.

3. Results and discussion

3.1. Qualitative analysis

Fig. 3 shows the contour evolution of transient temperature, pollutant concentration, and streamlines of a typical DNS run with $Fr_T = 2.0$, Re = 200, and $N = 3.0$ at six moments. As demonstrated, heat and pollutant concentration at the bottom, especially around the vent, decreased as the low-temperature fresh air passed the inlet port. The temperature and pollutant concentration profiles can be divided into three section: (1) the high temperature and pollutant concentration stage (top layer), (2) the intermediate stage where temperature and concentration decreases linearly to the bottom layer, and (3) the low temperature and pollutant concentration stage (bottom layer). The sequences of temperature and pollutant concentration profiles indicated that the height of the bottom layer

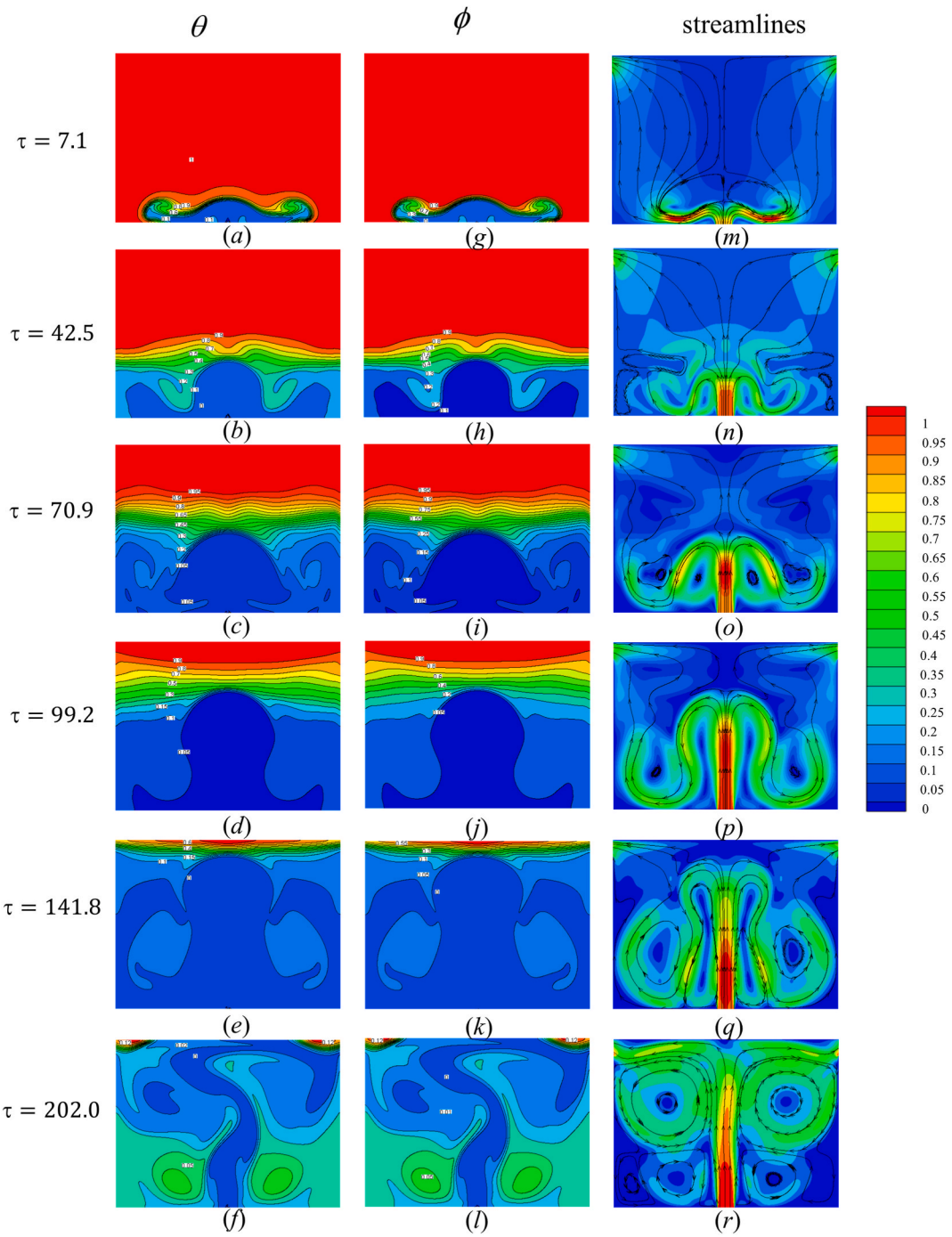

Fig. 3. Transient contours of temperature (left column), pollutant concentration (middle column), and streamlines (right column), wherein Fr_T = 2.0, Re = 200, and N = 3.0. Herein, temperature (θ) and pollutant concentration (φ) were non-dimensionalized with $(T - T_0)/(T_a - T_0)$ and $(C–C_0)/(C_a– C_0)$, while τ was non-dimensionalized with X_0/V_0.

increased and the cavity was filled by fresh air until the steady state, with pollutant discharged.

Fig. 4 shows the isotherms and iso-concentrations in the case of Fr_T = 2.0, Re = 200, and N = 3.0 at different heights, y = Y/H (0.03, 0.1, 0.2, 0.3, 0.4, 0.5, 0.6, 0.7, 0.8, and 0.9).

As observed, the fresh air supply at the early stage, the indoor temperature and the pollutant concentration decreased monotonously, while the decreasing rates decreased. As the airflow reached full development, the dimensionless temperature and pollutant concentration remained basically unchanged, indicating that heat and pollutant had been completely removed at this height, as

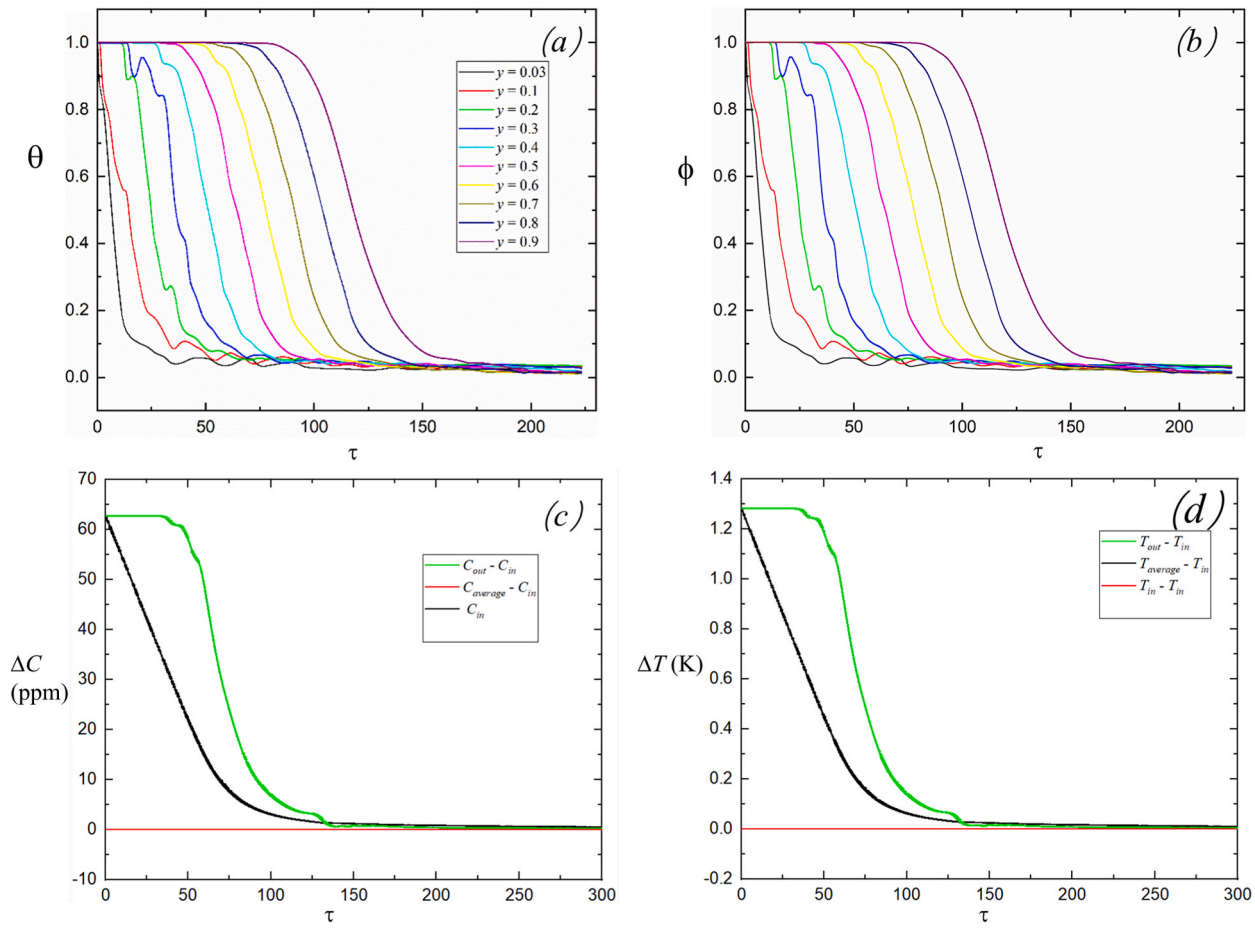

Fig. 4. Time series of temperature (a) and pollutant concentration (b) at different heights with $Fr_T = 2.0$, Re = 200, and $N = 3.0$, and the time series of temperature difference (c) and pollutant concentration difference (d) at indoor inlet port and outlet port with temperature (θ), pollutant concentration (φ) being non-dimensionalized with $(T - T_0)/(T_a - T_0)$, $(C–C_0)/(C_a– C_0)$, and τ being non-dimensionalized with X_0/V_0.

illustrated in Fig. 4 (a) and (b). As illustrated in Fig. 4 (c) and (d), the time series of temperature and pollutant concentration of indoor inlet port and outlet port. Such results confirmed the results shown in Fig. 3.

3.2. Quantitative analysis

As air pollutant and heat are closely related to each other owing to the shared source, the ventilation effectiveness for temperature distribution ε_t is equal to that for pollutant removal ε_c, hereinafter referred to as the ventilation effectiveness ε.

For each DNS run, a time series of ventilation effectiveness could be determined based on the results of direct numerical simulation. Fig. 5 shows four examples of such time series in cases of different *Re*, *N*, and Fr_T. At the early stage of inlet airflow, the ventilation effectiveness increased monotonously, while the increasing rate decreased gradually until the maximum ventilation effectiveness was reached at the dimensionless moment τ. As the airflow reached full development, the ventilation effectiveness remained unchanged, indicating that heat and pollutant of the whole room, at the inlet port, and at the outlet port were consistent, suggesting that heat and pollutants were completely removed at this height. Additionally, Fig. 5 (a)–(b) and (c)-(d) shows that the ventilation effectiveness in all DNS runs exceeded 1.0 as the temperature and pollutant concentration at the outlet were higher than those at the inlet, resulting in mixing and entrainment of heat and pollutant between the fresh airflow supply from inlet, the room airflow and the outlet airflow.

3.2.1. Effect of N (contaminant source intensity)

Fig. 6 shows the numerical results at $0.1 \leq N \leq 10.0$, $Fr_T = 2.0$, and Re = 100. As observed, the indoor airflow moved by following a double vortex pattern (one counterclockwise and one clockwise). At the full development stage, the thermal buoyancy force was greater than the solutal buoyancy force, wherein the indoor airflow was driven by thermal natural convection. The gradient of pollutant concentration decreased, while the temperature gradient increased. As a result, the indoor air velocity decreased as the buoyancy negative ratio N increased. The maximum temperature and pollutant concentration were observed at the roof, while temperature and pollutant concentration at the floor were more uniformly distributed. When $N > 1.0$, the solutal buoyancy force was

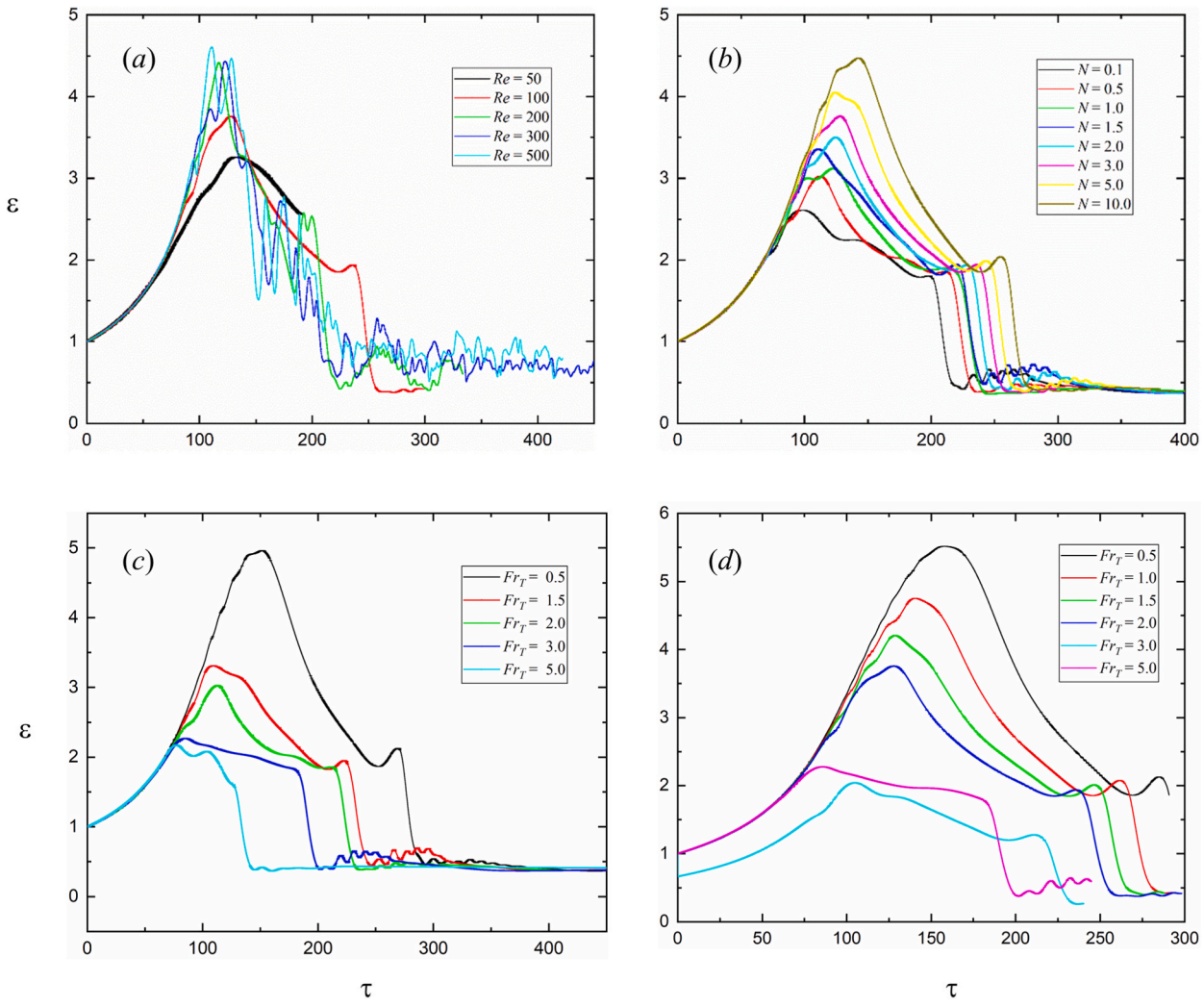

Fig. 5. Time series of ventilation effectiveness at $Fr_T = 2.0$, $N = 3.0$, $50 \leq Re \leq 500$ (a), $Fr_T = 2.0$, Re = 100, $0.1 \leq N \leq 10.0$ (b), Re = 100, $N = 0.5$, $0.5 \leq Fr_T \leq 5.0$ (c), Re = 100, $N = 3.0$, $0.5 \leq Fr_T \leq 5.0$ (d), wherein τ was non-dimensionalized with X_0/V_0.

greater than the thermal buoyancy force, the movement of air-pollutant mixture was induced by the solutal buoyancy force. This can be attributed to the fact that as the buoyancy ratio N increased, the pollutant buoyancy increased and the fluid movement was accelerated. Additionally, the isotherms and iso-concentrations were linearly stratified from top down. Overall, the indoor air quality can be improved by rationally increasing the pollutant concentration (within a reasonable range).

Fig. 9 (a) shows the ventilation effectiveness ε vs. *N* in all DNS runs. As observed, thet ventilation effectiveness increased as N increased, which can be attributed to the increase of negative buoyancy. The power-law fashion can be quantified by:

$$\varepsilon = 3.27303\, N^{0.12585} \tag{7}$$

wherein the regression coefficient was 0.9962.

3.2.2. *Effect of Fr (air supply temperature)*

Fig. 7 shows the numerical results at $0.5 \leq Fr_T \leq 5.0$, $N = 3.0$, and Re = 100. As *Fr* decreased, the ventilation effectiveness increased, and the magnitude of the stratified effect increased. This can be attributed to the fact that the negative buoyancy induced by both temperature and pollutant concentration increased as *Fr* decreased, resulting in reduced *Fr* and enhanced mixing and entrainment of the inlet airflow.

The dependence of ε on *Fr* can be quantified by:

$$\varepsilon = 3.58963 Fr^{-0.36} \tag{8}$$

wherein the regression coefficient was 0.96, as shown in Fig. 9(b).

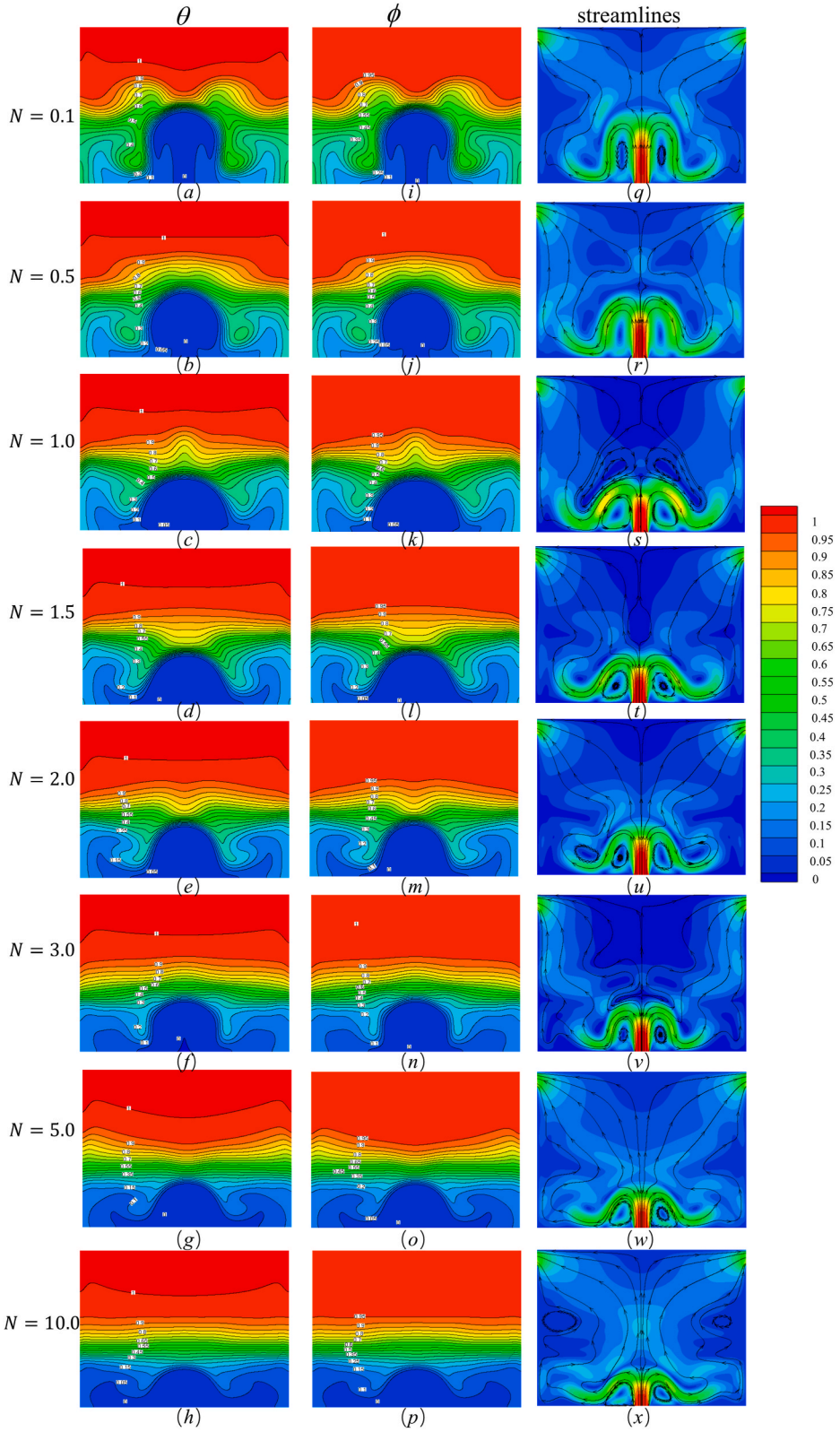

Fig. 6. Dimensionless isothermal (left), iso-concentrations (middle), and streamlines (right) at $0.1 \leq N \leq 10.0$, $Fr_T = 2.0$, and $\mathrm{Re} = 100$..

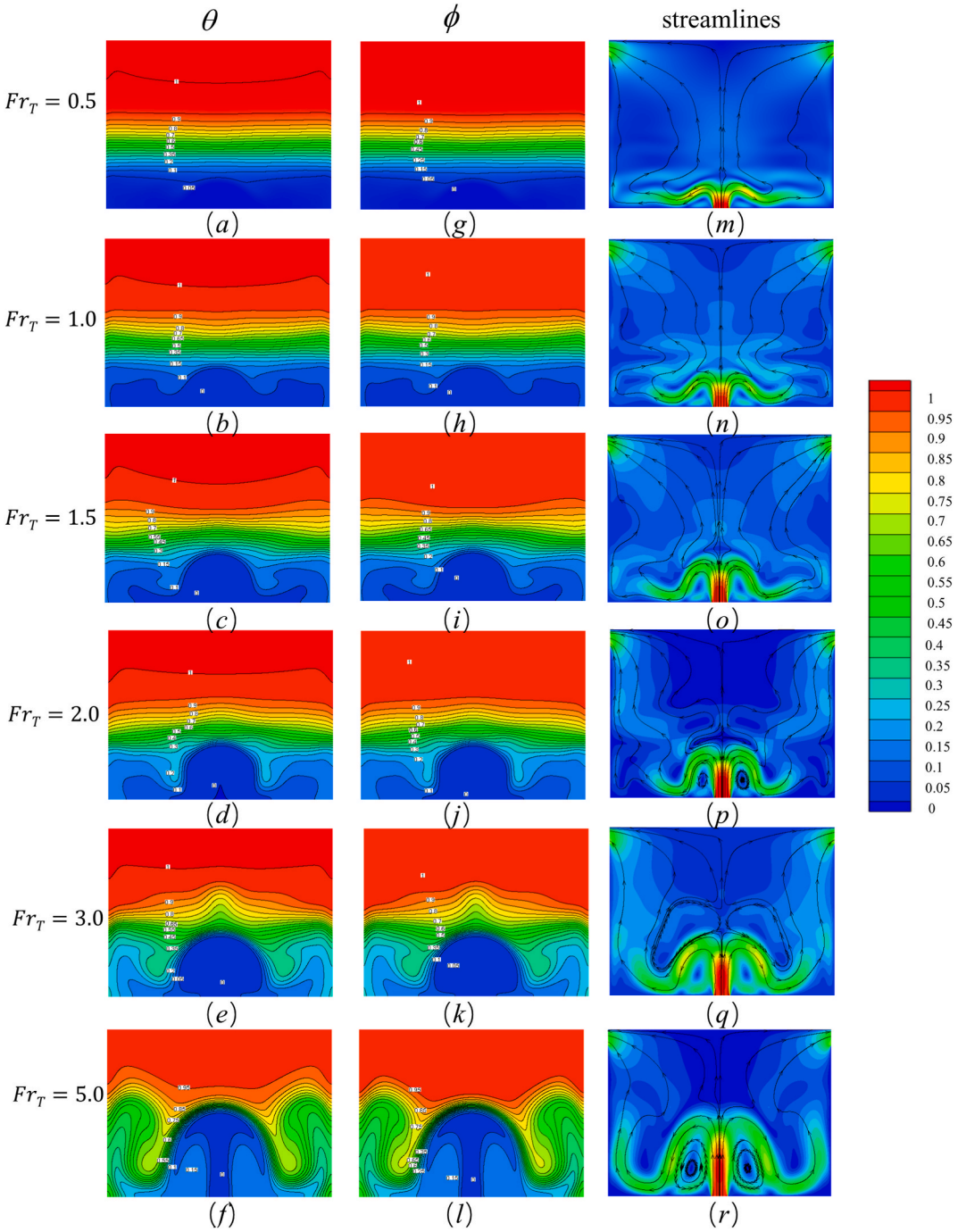

Fig. 7. Dimensionless isothermal (left column), iso-concentrations (middle column), and streamlines (right column) at $0.5 \leq Fr_T \leq 5.0$, $N = 3.0$, and $\mathrm{Re} = 100$.

3.2.3. *Effect of Re (air supply intensity)*

Fig. 8 illustrates the numerical results at $50 \leq Re \leq 500$, $Fr_T = 2.0$, and $N = 3.0$. In cases of $0.1 \leq N \leq 10.0$, the isotherms and isoconcentrations exhibited linear staratification from top down, with negligible entrainment of the inlet airflow into the core region of the room airflow. As a result, air-upflow and air-downflow were indistinguishable. When $Re \leq 50$, the indoor airflow was essentially double diffusion natural convection with coexistence of temperature and pollutant concentration effects. Additionally, indoor heat and pollutant stayed in the room for a long time, as shown in Fig. 8 (a), (g), and (l). At relatively large *Re*, as the air supply intensity increased, the core region of room was separated from the upflow, and the air jet height of floor air supply outlet also increased with

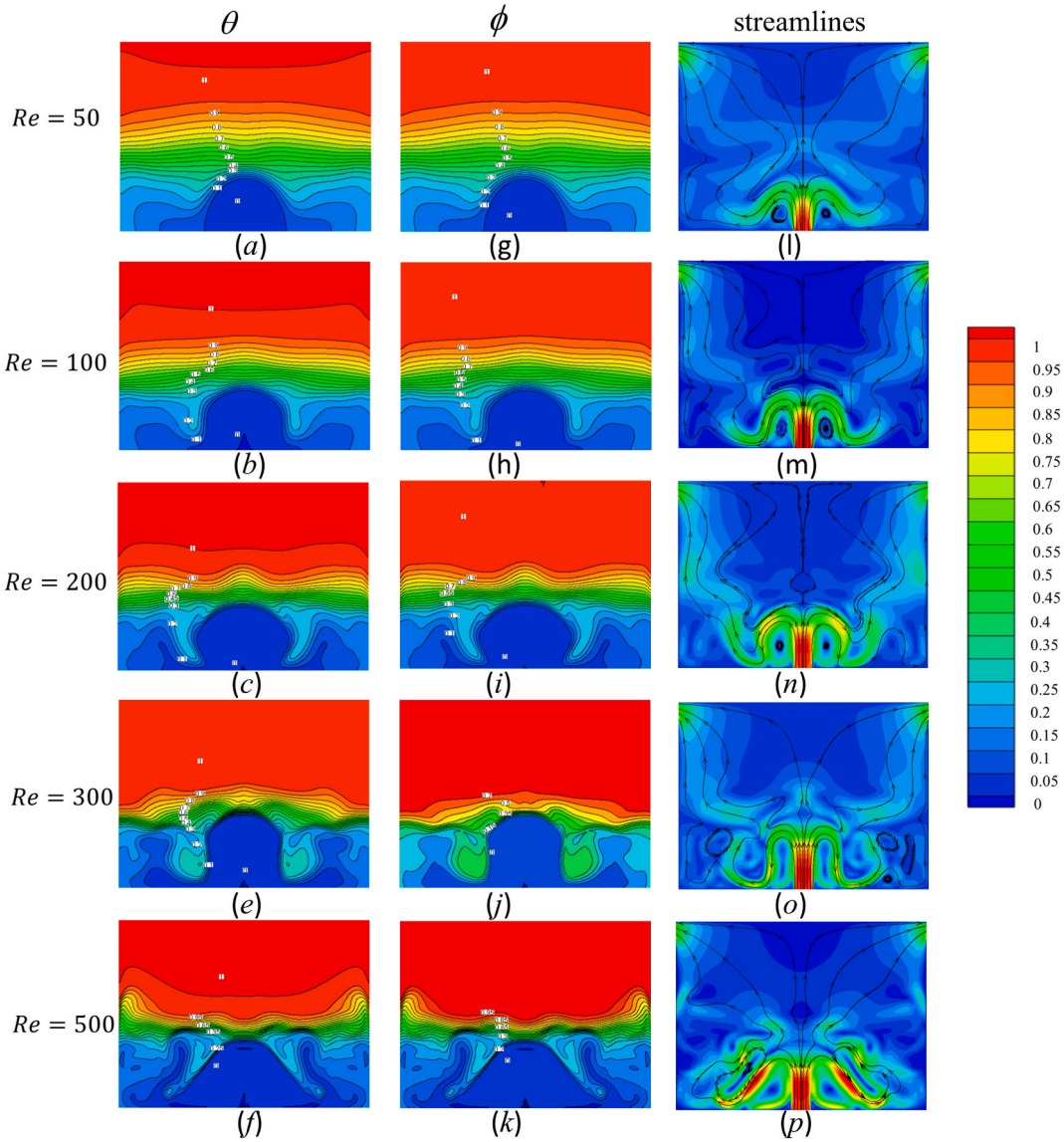

Fig. 8. Dimensionless isothermal (left column), iso-concentrations (middle column), and streamlines (right column) at $50 \leq Re \leq 500$, $N = 3.0$, and $Fr_T = 2.0$.

the air supply intensity.

The air supply velocity linearly decreased as room height increased, and the temperature difference would not cause the indoor wind speed to exceed the upper limit of 0.25 m/s recommended by ASHRAE.

As shown in Fig. 9(c), the influences of ε on Re can be obtained by:

$$\varepsilon = \begin{cases} 0.0075Re + 2.9342 & 50 \leq Re \leq 200 \\ 0.00002Re^2 - 0.0009Re + 4.511 & 200 < Re \leq 500 \end{cases} \tag{9}$$

where the coefficient was 0.9875 and 1.0, respectively.

As the dependence of ε on N, Fr, and Re can be obtained by the relations (7), (8) and (9), respectively. The combined effect of N, Fr and Re can be quantified by multivariable regression analysis:

$$\varepsilon = 0.36496Fr^{-0.08}Re^{0.39}N^{0.0024} + 1.28578 \tag{10}$$

where the regression coefficient was 0.98, as shown in Fig. 9 (d).

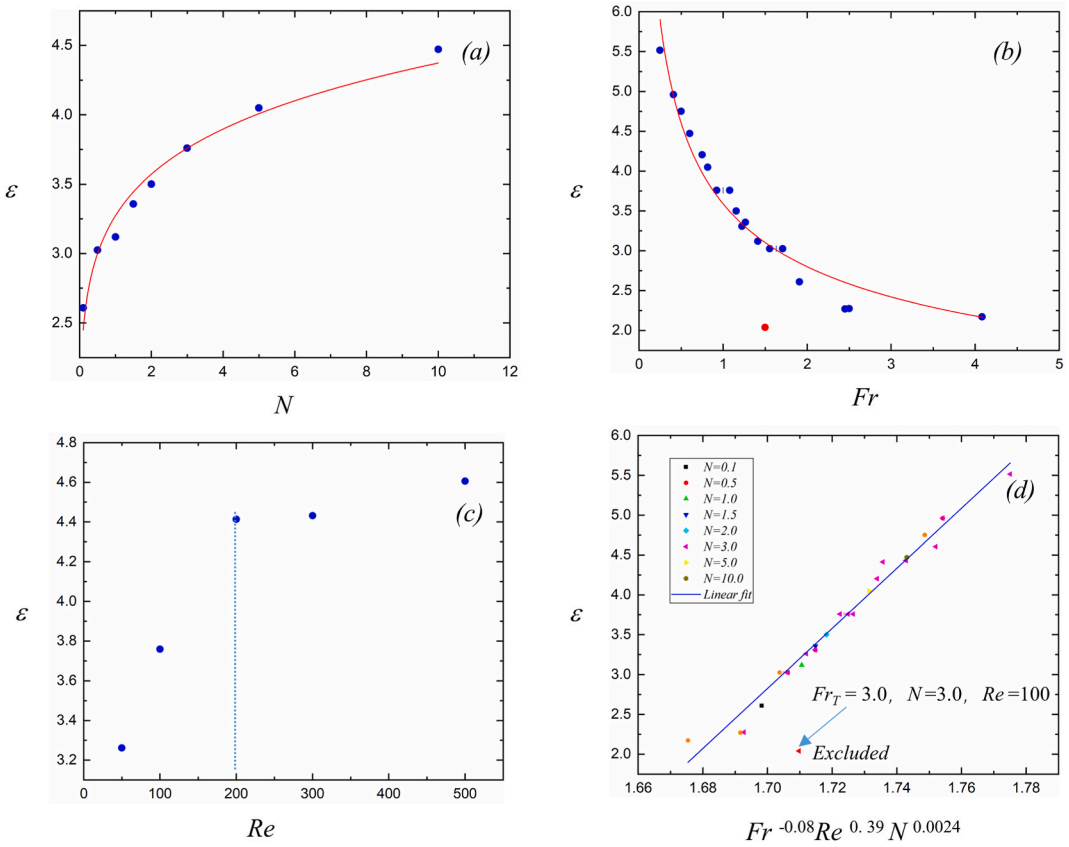

Fig. 9. (a) and (b) ε vs. N and *Fr*, respectively, (c) and (d) ε vs. *Re* and Fr-0.08*Re*0.39N0.0024, respectively.

4. Conclusions

Direct numerical simulations were conducted to investigate the UFAD systems, and explore the effects of *Re*, *Fr* and *N* on indoor air quality (IAQ) and ventilation effectiveness both qualitatively and quantitatively. As demonstrated, ε increased with Re and *N*, but decreased as *Fr* increased, ε was mainly influenced by *Re.* Stratifications of temperature and pollutant concentration were observed in all direct numerical simulations (DNS). Additionally, these feature parameters were significantly influenced by *Fr* and *Re*, although the effect of *N* was negligible and weaker than those of *Fr* and *Re.* This study provides references for preliminary design of UFAD systems.

Funding statement

The support from the National Natural Science Foundation of China (Grant No. 12362023) is gratefully acknowledged.

Data availability statement

Data will be made available on request.

CRediT authorship contribution statement

Yaowen Xia: Writing – review & editing, Writing – original draft, Visualization, Validation, Supervision, Software, Project administration, Methodology, Investigation, Formal analysis, Data curation, Conceptualization. **Saidong Lyu:** Writing – original draft, Validation.

Declaration of competing interest

The authors declare that they have no known competing financial interests or personal relationships that could have appeared to influence the work reported in this paper.

References

[1] Micheal A. William, et al., Evaluating heating, ventilation, and air-Conditioning Systems Toward Minimizing the airborne Transmission risk of Mucormycosis and COVID-19 Infections Built Environ. Case Stud. Thermal Eng. 28 (2021) 101567, https://doi.org/10.1016/j.csite.2021.101567.
[2] Ashraf Mimi Elsaid, M. Salem Ahmed, Indoor air quality strategies for air-conditioning and ventilation systems with the spread of the global coronavirus (COVID-19) epidemic: improvements and recommendations, Environ. Res. 199 (2021) 111314, https://doi.org/10.1016/j.envres.2021.111314.
[3] Roshanak Ashrafi, et al., The influence of covid related ventilation rate changes on the energy consumption and infection probability of the buildings: underfloor and overhead air distribution systems, Annual Modeling and Simulation Conf. (ANNSIM). IEEE, 2022 (2022), https://doi.org/10.23919/ANNSIM55834.2022.9859448.
[4] Lei Zhao, Junjie Liu, Jianlin Ren, Impact of various ventilation modes on IAQ and energy consumption in Chinese dwellings: first long-term monitoring study in Tianjin, China, Build. Environ. 143 (2018) 99–106, https://doi.org/10.1016/j.buildenv.2018.06.057.
[5] Chanjuan Sun, Zhiqiang Zhai, The efficacy of social distance and ventilation effectiveness in preventing COVID-19 transmission, Sustain. Cities Soc. 62 (2020) 102390, https://doi.org/10.1016/j.scs.2020.102390.
[6] Tariq Ahmed, Prashant Kumar, Laetitia Mottet, Natural ventilation in warm climates: the challenges of thermal comfort, heatwave resilience and indoor air quality, Renew. Sustain. Energy Rev. 138 (2021) 110669, https://doi.org/10.1016/j.rser.2020.110669.
[7] Arturs Staveckis, Anatolijs Borodinecs, Impact of impinging jet ventilation on thermal comfort and indoor air quality in office buildings, Energy Build. 235 (2021) 110738, https://doi.org/10.1016/j.enbuild.2021.110738.
[8] Ayman Alazazmeh, Muhammad Asif, Commercial building retrofitting: assessment of improvements in energy performance and indoor air quality, Case Stud. Therm. Eng. 26 (2021) 100946, https://doi.org/10.1016/j.csite.2021.100946.
[9] Ajith N. Nair, et al., A review of strategies and their effectiveness in reducing indoor airborne transmission and improving indoor air quality, Environ. Res. 213 (2022) 113579, https://doi.org/10.1016/j.envres.2022.113579.
[10] Nehul Agarwal, et al., Indoor air quality improvement in COVID-19 pandemic, Sustain. Cities Soc. 70 (2021) 102942, https://doi.org/10.1016/j.scs.2021.102942.
[11] Na Kyong Kim, et al., Airflow pattern control using artificial intelligence for effective removal of indoor airborne hazardous materials, Build. Environ. 204 (2021) 108148, https://doi.org/10.1016/j.buildenv.2021.108148.
[12] Xiaolei Fan, et al., Uniformity of supply air in the plenum for under-floor air distribution ventilation in a circular conference room: a CFD study, Energies 15 17 (2022) 6370, https://doi.org/10.3390/en15176370.
[13] Chang Heon Cheong, Beungyong Park, Seong Ryong Ryu, Effect of under-floor air distribution system to prevent the spread of airborne pathogens in classrooms, Case Stud. Therm. Eng. 28 (2021) 101641, https://doi.org/10.1016/j.csite.2021.101641.
[14] Kai Zhang, et al., Review of underfloor air distribution technology, Energy Build. 85 (2014) 180–186, https://doi.org/10.1016/j.enbuild.2014.09.011.
[15] S. Hui, Y.U.G.U.O. Li, Enhancing sustainability of buildings by using underfloor air conditioning systems, Proc. Chonqing-Hong Kong Joint Symp. (2002).
[16] Lounes Koufi, et al., Numerical investigation of turbulent mixed convection in an open cavity: effect of inlet and outlet openings, Int. J. Therm. Sci. 116 (2017) 103–117, https://doi.org/10.1016/j.ijthermalsci.2017.02.007.
[17] Jodelle Degois, et al., Indoor air quality assessment in dwellings with different ventilation strategies in Nunavik and impacts on bacterial and fungal microbiota, Indoor air 31 6 (2021) 2213–2225, https://doi.org/10.1111/ina.12857.
[18] Behrang Chenari, João Dias Carrilho, Manuel Gameiro da Silva, Towards sustainable, energy-efficient and healthy ventilation strategies in buildings: a review, Renew. Sustain. Energy Rev. 59 (2016) 1426–1447, https://doi.org/10.1016/j.rser.2016.01.074.
[19] Wenhua Chen, et al., Experimental and numerical investigations of indoor air movement distribution with an office ceiling fan, Build. Environ. 130 (2018) 14–26, https://doi.org/10.1016/j.buildenv.2017.12.016.
[20] Gon Kim, et al., Thermal comfort prediction of an underfloor air distribution system in a large indoor environment, Energy Build. 64 (2013) 323–331, https://doi.org/10.1016/j.enbuild.2013.05.003.
[21] Yuanda Cheng, Jianlei Niu, Naiping Gao, Stratified air distribution systems in a large lecture theatre: a numerical method to optimize thermal comfort and maximize energy saving, Energy Build. 55 (2012) 515–525, https://doi.org/10.1016/j.enbuild.2012.09.021.
[22] R. Tomasi, et al., Experimental evaluation of air distribution in mechanically ventilated residential rooms: thermal comfort and ventilation effectiveness, Energy Build. 60 (2013) 28–37, https://doi.org/10.1016/j.enbuild.2013.01.003.
[23] Meng Gao, et al., A study on thermal performance of a novel glazed transpired solar collector with perforating corrugated plate, J. Clean. Prod. 257 (2020) 120443, https://doi.org/10.1016/j.jclepro.2020.120443.
[24] Ali Alajmi, Wid El-Amer, Saving energy by using underfloor-air-distribution (UFAD) system in commercial buildings, Energy Convers. Manag. 51 (8) (2010) 1637–1642, https://doi.org/10.1016/j.enconman.2009.12.040.
[25] T.Y. Tsai, R.H. Liou, Y. Lin, An experimental study on the indoor environment using UnderFloor air distribution system, Procedia Eng. 79 (2014) 263–266, https://doi.org/10.1016/j.proeng.2014.06.341.
[26] I.S.M.A.I.L. Firas Basim, Thermal comfort analysis for overhead and underfloor air distribution systems, CFD Letters 13 (12) (2021) 113–132, https://doi.org/10.37934/cfdl.13.12.113132.
[27] Muntasir Alam, et al., Effect of location of a rotating circular cylinder and heat source on mixed convection heat transfer characteristics inside a square enclosure with discrete heater at the bottom wall, AIP Conf. Proc. 1851 (No. 1) (2017), https://doi.org/10.1063/1.4984730. AIP Publishing LLC.
[28] Gon Kim, et al., Thermal comfort prediction of an underfloor air distribution system in a large indoor environment, Energy Build. 64 (2013) 323–331, https://doi.org/10.1016/j.enbuild.2013.05.003.
[29] Sung-Woo Ryu, Doo-Yong Park, Effect of blind angles on thermal decay in the UFAD system in summer, Appl. Therm. Eng. (2022) 118927, https://doi.org/10.1016/j.applthermaleng.2022.118927.
[30] Peng-Yi Cui, Zhuo Li, Wen-Quan Tao, Buoyancy flows and pollutant dispersion through different scale urban areas: CFD simulations and wind-tunnel measurements, Build. Environ. 104 (2016) 76–91, https://doi.org/10.1016/j.buildenv.2016.04.028.
[31] Xiumin Dou, et al., Improved buoyancy-driver hybrid ventilation system for multiple-heat-source industrial buildings, Case Stud. Therm. Eng. 26 (2021) 101059, https://doi.org/10.1016/j.csite.2021.101059.
[32] Yi-Jiun Peter Lin, P.F. Linden, A model for an under floor air distribution system, Energy and Buildings 37 (4) (2005) 399–409, https://doi.org/10.1016/j.enbuild.2004.07.011.
[33] Q.A. Liu, P.F. Linden, The fluid dynamics of an underfloor air distribution system, J. Fluid Mech. 554 (2006) 323–341, https://doi.org/10.1017/S0022112006009414.
[34] Y.J.P. Lin, T.Y. Tsai, An experimental study on a full-scale indoor thermal environment using an Under-Floor Air Distribution system, Energy Build. 80 (2014) 321–330, https://doi.org/10.1016/j.enbuild.2014.05.028.
[35] Mohamad Kanaan, Modelling of contaminant dispersion in underfloor air distribution systems: comparison of analytical and CFD methods, J. Building Performance Simulation 12 (6) (2019) 759–769, https://doi.org/10.1080/19401493.2019.1655096.
[36] Aminhossein Jahanbin, Efficacy of coupling heat recovery ventilation and fan coil systems in improving the indoor air quality and thermal comfort condition, Energy and Built Environ. 3 (4) (2022) 478–495, https://doi.org/10.1016/j.enbenv.2021.05.005.
[37] Jungsuk Lee, et al., Effect of air cleaner on reducing concentration of indoor-generated viruses with or without natural ventilation, Aerosol Sci. Technol. 55 (11) (2021) 1288–1303, https://doi.org/10.1080/02786826.2021.1945528.
[38] J. Serrano-Arellano, et al., Numerical investigation of transient heat and mass transfer by natural convection in a ventilated cavity: outlet air gap located close to heat source, Int. J. Heat Mass Tran. 76 (2014) 268–278, https://doi.org/10.1016/j.ijheatmasstransfer.2014.04.055.
[39] Bin Yang, et al., A review of advanced air distribution methods-theory, practice, limitations and solutions, Energy Build. 202 (2019) 109359, https://doi.org/10.1016/j.enbuild.2019.109359.

[40] Zohir Younsi, Lounes Koufi, Hassane Naji, Numerical study of the effects of ventilated cavities outlet location on thermal comfort and air quality. International Journal of Numerical Methods for Heat & Fluid Flow, 2019, https://doi.org/10.1108/HFF-09-2018-0518.
[41] Peng, Yong Xiao, et al., Numerical simulation on effects of air supply angle and air supply velocity to indoor thermal environment of wall hanging air-conditioning, Adv. Mater. Res. 1030 (2014). https://doi.org/10.4028/www.scientific.net/AMR.1030-1032.553. Trans Tech Publications Ltd.
[42] Sumei Liu, et al., Improving indoor air quality and thermal comfort in residential kitchens with a new ventilation system, Build. Environ. 180 (2020) 107016, https://doi.org/10.1016/j.buildenv.2020.107016.
[43] Man Fan, et al., A review of different ventilation modes on thermal comfort, air quality and virus spread control, Build. Environ. (2022) 108831, https://doi.org/10.1016/j.buildenv.2022.108831.
[44] Jie Gao, et al., Indoor air distribution in a room with underfloor air distribution and chilled ceiling: effect of ceiling surface temperature and supply air velocity, Indoor Built Environ. 29 (2) (2020) 151–162, https://doi.org/10.1177/1420326X19853605.
[45] Kai Zhang, et al., Simplified model for desired airflow rate in underfloor air distribution (UFAD) systems, Appl. Therm. Eng. 93 (2016) 244–250, https://doi.org/10.1016/j.applthermaleng.2015.09.053.
[46] I. Sezai, A.A. Mohamad, Double diffusive convection in a cubic enclosure with opposing temperature and concentration gradients, Phys. Fluids (9) (2000) 2210–2223, https://doi.org/10.1063/1.1286422.
[47] Lounes Koufi, et al., Double-diffusive natural convection in a mixture-filled cavity with walls' opposite temperatures and concentrations, Heat Transfer Eng. 40 (15) (2019) 1268–1285, https://doi.org/10.1080/01457632.2018.1460928.
[48] J. Xamán, et al., Optimum ventilation based on the overall ventilation effectiveness for temperature distribution in ventilated cavities, Int. J. Thermal Sci. 48 (8) (2009) 1574–1585, https://doi.org/10.1016/j.ijthermalsci.2008.12.008.
[49] C. Beghein, F. Haghighat, F. Allard, Numerical study of double-diffusive natural convection in a square cavity, Int. J. Heat and Mass Transfer 35 (4) (1992) 833–846, https://doi.org/10.1016/0017-9310(92)90251-M.